Message 1 of 1

Sent at: 10/08/2020 09:33:33

Fw: Congratulations! Your article has been published in the Early Access area on IEEE Xplore

From: Alberto Reatti <alberto@reatti@unifi.it>
To: Prof Alberto Reatti <alberto.reatti@unifi.it>

From: Antonio Faba <antonio.faba@unipg.it>
Date: 09/08/2020 20:43:04
Subject: Fw: Congratulations! Your article has been published in the Early Access area on IEEE Xplore
To: Ermanno Cardelli <ermanno.cardelli@unipg.it>, Alberto Reatti <alberto.reatti@unifi.it>, Fabio Corti <fabio.corti@unifi.it>, Hari Rimal <haririmal@ioe.edu.np>, simonequondam87@gmail.com <simonequondam87@gmail.com>

Salve a tutti,

L'articolo è stato pubblicato come early access.

Antonio

Antonio Faba
University of Perugia - Dep. of Engineering
Polo Scientifico Didattico di Terni
Strada di Pentima, 4 - 05100 TR - Italy
+39 0744 492912

Da: wmsprod@ieee.org <wmsprod@ieee.org>
Inviato: domenica 9 agosto 2020 01:31
A: Antonio Faba <antonio.faba@unipg.it>
Oggetto: Congratulations! Your article has been published in the Early Access area on IEEE Xplore

Dear Dr. Antonio Faba

This is to notify you that the following article, "Protection from Indirect Lightning Effects for Power Converters in Avionic Environment: Modelling and Experimental Validation," is available under the "Early Access" area on IEEE Xplore. This article has been accepted for publication in a future issue of this journal, but has not been edited and content may change prior to final publication. It may be cited as an article in a future issue by its Digital Object Identifier. To view this article, please visit the journal homepage (listed below) on IEEE Xplore and select the ?Early Access? tab.

This paper appears in: IEEE Transactions on Industrial Electronics

On page(s): 0
Print ISSN: 0278-0046
Online ISSN: 1557-9948
Digital Object Identifier: 10.1109/TIE.2020.3013794

Protection from Indirect Lightning Effects for Power Converters in Avionic Environment: Modelling and Experimental Validation

Hari Prasad Rimal, *Student Member, IEEE*, Alberto Reatti, *Member*, *IEEE*, Fabio Corti, Student *Member*, *IEEE*, Gabriele Maria Lozito, *Member*, *IEEE*, Simone Quondam Antonio, Antonio Faba, *Senior Member, IEEE,* and Ermanno Cardelli, *Senior Member, IEEE*

***Abstract*—This paper focuses on a protection system from lightning indirect effects applicable to power converters for avionic applications. The case-study considered in this paper is a DC-DC PWM Buck-Boost converter protected by a metal oxide varistor and a series inductive blocking element. The converter is investigated when operated a) in normal operating conditions, b) under lightning indirect strokes without protection, and c) under lightning indirect strokes with protection. A numerical model of the system based on a finite-difference-time-domain scheme is proposed. Validation of the system is performed through a comparison with experimental measurements and alternative numerical modeling techniques, showing the effectiveness of the blocking system and the accuracy of the proposed model.**

***Index Terms*—Power Conversion, Aircraft lightning effects, Varistors, Inductors, Numerical Analysis.**

I. INTRODUCTION

THE modern avionic sector is becoming more and more electrical in the sense that modern electrical equipment is replacing the classical mechanical one [1]. The selection of electrical equipment over the mechanical is a tradeoff between the functionality over the robustness. Among the electrical equipment involved in this trend, PWM DC-DC power converters are crucial. They are simple well-known circuits [2-4], and even if they are widely investigated [5-6], several issues are still open and challenging for research and application. A fundamental requirement for power converters is their ability to regulate the output voltage, keeping its value constant under all operating conditions, including transients to ensure the overall supplied system stability [7-10]. Especially in avionics, the reliability of the converter circuit becomes a mandatory issue to be considered [11], so the severe transient condition viz. lightning indirect effects must be investigated during the design phase. The evaluation of the converter dynamic response is useful to estimate its reliability and to evaluate its performance [12-13]. A widely and commonly used evaluation method for the lightning indirect effects is the test of the equipment by using the waveforms given by the international standard for avionic applications [14-15]. The RTCA/DO-160G is one of the most used standards to establish the airworthiness of aircraft during the lightning strokes [16]. The above cited standard proposes different voltage and current waveforms, pulses or damped sinusoids, with different amplitudes and different coupling methods, for different scenarios where the equipment under test will be installed. For instance, the position inside the aircraft, the distances from the shielding apertures, the cables length, the cable types (shielded or not) etc. In this paper we propose a protection device for equipment that mostly has to withstand slow waveforms called 4/1 and 5A/5A. The analysis is done using those transients to determine the voltage and current levels on the power converter components during typical indirect lightning phenomena. Sometimes these levels can overcome the safety limits of the components, and the effects are temporary faults or permanent damages [17]. For these reasons, during the design stage of the converter, it is very important to simulate the indirect lightning effects and check the corresponding immunity levels [18-19]. When the test severity overcomes the strength of the converter components, a suitable protection device must be used [20]. In this paper, the effects of indirect lightning pulses on a PWM DC-DC power converter are modeled, and a suitable protection system consisting of the combination of a series Blocking Inductor (BI) and a Metal Oxide Varistor (MOV) is designed and tested. This configuration has been previously presented and studied in [21] in a standalone configuration. It can protect sensible devices that require low clamping voltage during severe lightning phenomena. This combined filter exploits the damping effect of the BI to mitigate the pulse current in the MOV with low clamping voltage. Effectiveness of the protection system is strictly dependent on the equivalent impedance of the Equipment Under Test (EUT). The analysis presented in [21] with the proposed protection device was not complete rather partial, because the EUT was a simple linear and time-invariant dipole. In this paper, the BI-MOV protecting device is tested in combination with a real PWM DC-DC converter, which results to be a non-linear and time-varying EUT. This work completes the analysis started in [21] proving the method reliability and effectiveness for an operative case, useful from the practical point of view. A typical PWM DC-DC Buck-Boost (BUBO) power converter is selected for the evaluation of the effectiveness and the reliability of this technique in the avionic environment, because it provides an output voltage, which cane both higher and lower than the input voltage. The system under study is simulated using the Finite Difference Time Domain (FDTD) numerical scheme. This study also provides the basic guideline to design the BI-MOV combination to meet the constraint of space and payload for the onboard equipments. The results computed by using the FDTD approach are compared with those obtained from the State Space Approach (SSA) implemented in commercial codes like MATLAB/SIMULINK©, and, also, with those derived via dedicated circuit simulation environment such as LTspice©, for some basic test cases. The effects of non-linearity, switching transients, and parasitic components are taken into consideration. A prototype of a BUBO converter with the combined BI-MOV

has been built, and the computed results validated by means of dedicated experimental tests using a standard lightning generator for lightning indirect effects in avionics [16].

II. DC-DC BUBO CONVERTER DESIGN

A DC-DC BUBO converter circuit is shown in the Fig. 1(i). It consists of a power switch *Q* (MOSFET), a diode *D*, an inductor *L*, with its equivalent series resistance R_L, and an output capacitor *C*. The voltage generator V_{in}, the inductance L_i and the resistance R_i model the input test voltage pulse to the converter circuit, and *R* is the load resistor. Fig. 1(ii) presents the equivalent circuital model of the power switch *Q* and diode *D* used to perform the switched simulation of the circuit depicted in Fig. 1(i). In Fig. 1(ii), the switch S_1, the resistance *Rs* and the inductance *Ls* model the power MOSFET, similarly, the switch S_2, the voltage generator V_F and the resistance *Rd* model the diode. Assuming a Continuous Conduction Mode (CCM) operation for the converter circuit, and according to the design procedure given in [7], the minimum inductance *L* can be calculated as

$$L_{\min} = \frac{R_L^{\max}(1-D_{\min})^2}{2f_S} \tag{1}$$

where, R_L^{max} is the maximum value of the load resistance, D_{min} is minimum duty cycle the converter is operated at, and f_S is switching frequency. Assuming R_L^{max} to be 50Ω, and D_{min} to be 0.2, the inductance minimum value is L_{min} = 160µH. The minimum value of capacitance *C* that ensure a ripple lower than ΔV_C is given by

$$C_{\min} = \frac{V_O^{\max} D_{\max}}{f_S \Delta V_C R_{\min}} \tag{2}$$

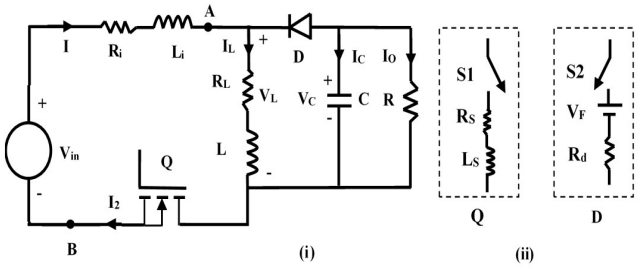

Fig. 1. (i) Schematic diagram of the DC-DC BUBO Converter, (ii) adopted circuital model of power Mosfet (Q) and diode (D).

where, V_o^{max} is the maximum output voltage, D_{max} is the maximum value of duty cycle and R_{min} is the minimum value of load resistance. Assuming D_{max}=0.8, R_{min}=50 Ω, then, $V_o^{max} = V_i D_{max}/(1-D_{max}) = 48$V. To ensure a maximum ripple ΔV_C of 200 mV, filtering capacitance *C* must be larger than C_{min} = 38.4µF; *C* = 66µF is selected. The inductor has been assembled by winding 38 turns of a 40AWG *Litz* wire on a Yuxiang©, model ETD39 N77 core with two air gaps of 0.2 mm each. *Litz* wire has been used to reduce skin and proximity effect at switching frequency f_S of 100 kHz. According to currents and voltage stress values, a Vishay© IRF740 power MOSFET, with a drain to source breakdown voltage V_{DS} = 400V, and a continuous current at 25°C I_D=10A has been selected. Similarly, a Panjit© model SB140 diode with a maximum DC blocking voltage V_{DC}=40V and a maximum average forward rectified current $I_{F(AV)}$=1A has been selected. The converter components parameters are listed in Table I.

III. MODELLING OF THE DC-DC BUBO CONVERTER AND THE SIMULATION OF THE INDIRECT LIGHTNING EFFECTS

The switching sequence applied to the switches S_1 and S_2 of the BUBO converter are in the logical NOT to each other. Moreover, the parasitic capacitance of the BUBO inductor C_P is considered. The direction of the different branch currents and the polarity of the voltages are positive according to Fig. 1. The quantities of interest obtained from the simulations are current and voltage of the converter components. Usually, the normal BUBO operation is achieved assuming V_{in} as a DC voltage source, whereas, in this paper, the input source generates several waveforms according to RTCA/DO-160G to evaluate the indirect lightning effects [16].

A. FDTD approach

The CCM operation of the converter is based on two states alternating in the time: *S_1 ON - S_2 OFF* and *S_1 OFF - S_2 ON*. The application of Kirchhoff's voltage and current law for these two states results in the following volt-amp balance equations

$$V_{in} - (R_i + R_s)I - (L_i + L_s)\frac{dI}{dt} - V_L = 0 \tag{3}$$

$$V_L - R_L I_L - L\frac{dI}{dt} = 0 \tag{4}$$

$$V_C + RC\frac{dV_C}{dt} = 0 \tag{5}$$

$$I - I_L - C_P\frac{dV_L}{dt} = 0 \tag{6}$$

$$V_C + RI_L + RC_P\frac{dV_L}{dt} + RC\frac{dV_C}{dt} = 0 \tag{7}$$

$$V_C - V_F - R_d I_L - R_d C_P\frac{dV_L}{dt} - V_L = 0 \tag{8}$$

$$I = 0 \tag{9}$$

where (3) to (6) represent the *S_1 ON - S_2 OFF* state of the circuit, whereas (4) and (7)-(9) are valid for the *S_1 OFF- S_2 ON* state of the circuit. Equations (3)-(9) can be discretized using the Crank Nicholson algorithm in the FDTD scheme [22]. The solution of the system yields the four quantities *I*, I_L, V_L and V_C, where V_L is the voltage across the inductor parasitic capacitance C_P. The other quantities viz. the switches voltages and currents are derived from these four quantities. Switches S_1 and S_2 must conduct only in the forward direction as indicated by the arrowhead, this is obtained by an external control.

B. State Space approach

The converter time-domain response is determined by integrating the state equations of the circuit. Since the converter can be represented in two operating conditions, *S_1 ON* and *S_1 OFF*, one sets of state equations is formulated each condition. The state variables are the currents on all inductors and the voltages across all capacitors, including the parasitic elements. The *S_1 ON* and *S_1 OFF* circuits with the numbered state variables are shown in Fig. 2, where the total input resistance is $R_{in}=(R_i+R_s)$, the total input inductance is $L_{in}=(L_i+L_s)$, and the current-controlled current generator, represnting the the diode non-linear characteristic is

$$I_D = \min\left(0, \frac{x_1 - V_F - x_3}{R_d}\right) \tag{10}$$

where V_F is the diode forward voltage and R_d is the diode series resistance. The state equations for the two operating conditions are

$$S1\,ON:\begin{cases}\dot{x}_1=\frac{1}{C}\left(-\frac{x_1}{R}-I_D\right)\\ \dot{x}_2=\frac{1}{L}\left(x_3-R_L x_2\right)\\ \dot{x}_3=\frac{1}{C_P}\left(x_4-x_2+I_D\right)\\ \dot{x}_4=\frac{1}{L_{in}}\left(V_{in}-R_{in}x_4-x_3\right)\end{cases}\qquad S1\,OFF:\begin{cases}\dot{x}_1=\frac{1}{C}\left(-\frac{x_1}{R}-I_D\right)\\ \dot{x}_2=\frac{1}{L}\left(x_3-R_L x_2\right)\\ \dot{x}_3=\frac{1}{C_P}\left(-x_2+I_D\right)\end{cases}\qquad (11)$$

The time-domain evolution is computed through the forward Euler method. For the k-th state variable we have

$$x_k\left(t+\tau\right)=x_k(t)+\dot{x}_k(t)\cdot\tau \qquad (12)$$

According to the state of the switches, the correct set of equations are used to compute the time domain evolution of the converter. The state variable x_4 is not present in the S_1 *OFF* operating condition (since the open-circuit switch is in series with the relative L_{in} inductor), and for this reason, it is directly forced to zero in this state.

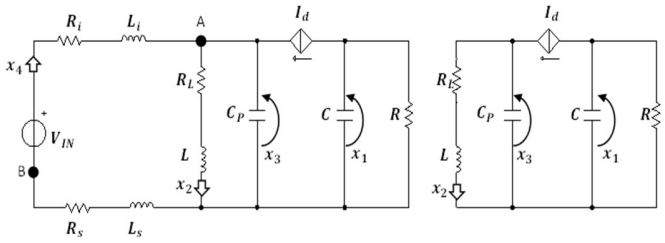

Fig. 2. Circuit for operating conditions. S1 ON left, S1 OFF right.

C. Indirect Lightning Effects and the Response of the Power Converter

The direct lightning current stroke to the outer skin of the aircraft creates a time changing magnetic field. This magnetic field induces a transient voltage in the wirings of the onboard electrical equipment. This induced transient voltage can upset or damage the electronic equipment onboard the aircraft, the phenomenon is commonly known as indirect lightning effect. The standard [16] used in this study defines the combination of various types of waveforms and the test procedures, in particular, the Fig. 3 shows the unipolar double exponential voltage/current pulse that is used for the paper purpose. Waveform 4/1 and waveform 5A/5A with amplitudes ranging from level 1 to level 5 are defined for the pin injection test procedure. They are relatively slow rising transient waveforms as compared to the other waveforms considered in the standard. Depending upon the amount of electromagnetic shielding and the type of electromagnetic coupling viz. structure coupling, aperture coupling, etc., each equipment must comply with different amplitudes of these waveforms. The waveforms of the appropriate wave shape and amplitudes are modelled using the parameters given in Table II.

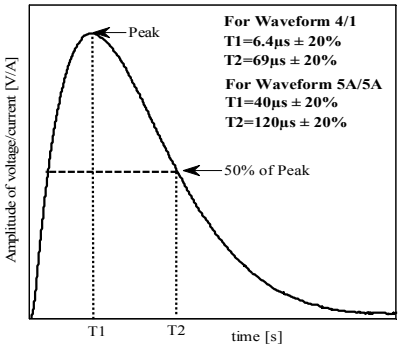

Fig. 3. Double exponential waveform 4/1 and waveform 5A/5A.

The response of power converter to the lightning waveforms can be determined, for instance, by using the approach mentioned in the sub-section A, where, V_{in} in (3) is the indirect lightning voltage, R_i and L_i are the lightning generator internal resistance and inductance, respectively. Figures 4, 5 and 6 present the current and voltage along the BUBO converter MOSFET, Diode, inductor, and output capacitor, upon the application of the level 4 amplitude of the waveform 5A/5A. The absolute maximum voltage limit and the current limit (dashed red lines) of the prototype converter components used in this study are specified in the same figures. It is evident that the components current and voltage limits are easily exceeded during the lightning stroke. The level 4 amplitude is one of the most severe transient amplitude the EUT should qualify for, and this is the reason it has been selected to predict the response of the converter. Experimental measurements have not been performed in that case because the power converter components would have been certainly damaged or destroyed.

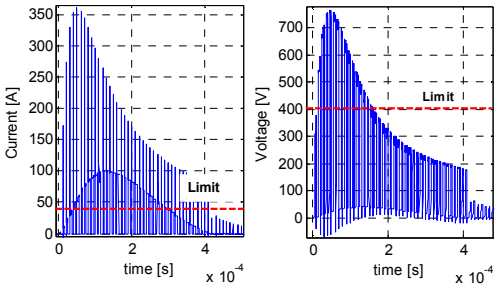

Fig. 4. Mosfet current (left) and Mosfet voltage (right) during the transient waveform 5A/5A level 4 (FDTD simulation).

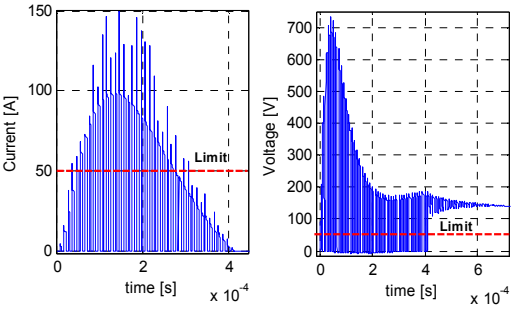

Fig. 5. Diode current (left) and Diode voltage (right) during transient waveform 5A/5A level 4 (FDTD simulation).

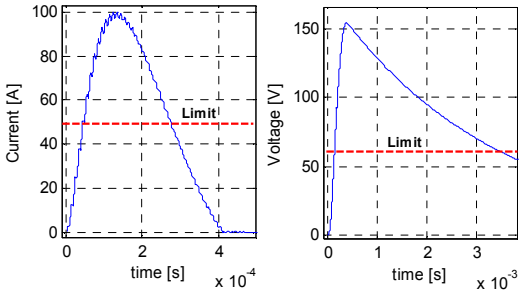

Fig. 6. BUBO inductor current (left) and output capacitor voltage (right) during the transient waveform 5A/5A level 4 (FDTD simulation).

IV. Lightning Protection Of The Power Converter: Simulation And Design

The simulation results shown in III.C predicts that the voltage and current across the elements of the power converter exceed their safety limits during lightning events. The use of a robust and efficient protection system is mandatory to ensure the uninterrupted operation of the converter during such lightning strokes. The MOV is the most frequently used protection device, therefore, it has been selected for this study.

A. Power Converter protected by MOV: Modeling and simulation.

The MOV is connected across the point *A-B* of the BUBO converter reported in Fig.1(i) to protect the converter from indirect lightning; in such configuration it is able to protect the downstream components due to its capability to sink a larger share of the transient current [23]. The MOV is modelled as a non-linear resistance R_m with a parasitic capacitance C_m in parallel [24]. The parameter C_m is specified in the varistor datasheet e.g. for EPCOS©, it is generally specified for 100 kHz [25]. The non-linear resistance R_m is calculated as follows,

$$R_m^{n+1} = K_i * V_{ref} * \left(I_V^n\right)^{(g-1)} * \left(\frac{1}{I_{ref}}\right)^g . \quad (13)$$

$$g = \frac{1}{\alpha_i}$$

where, V_{ref} is the reference voltage specified in the datasheet at a reference current I_{ref}=1 mA, I_V is the current passing through the non-linear resistor R_m. The non-linear Volt-Amp characteristic of the MOV is divided into three regions, each having its unique set of values for parameters K and α [26]. The values of K and α for three regions are evaluated from the measured clamping voltage and the varistor current. The deviation between measured and calculated R_m is minimized to determine the value of K and α. The value of R_m for $n+1$ time step during the simulation is calculated using the current through R_m i.e. I_V in the n^{th} time step. Parameters K, α, V_{ref} *and* I_{ref}, the model and the manufacturer of the MOV are specified in Table III. For the circuit reported in Fig.1(i), after the insertion of the MOV across *A-B*, the application of Kirchhoff voltage and current laws (*KVL, KCL*) results in the volt-amp balance equations reported below.

$$V_{in} - I R_i - L_i \frac{dI}{dt} - I_V R_m = 0 \quad (14)$$

$$V_E - I_V R_m = 0 \quad (15)$$

$$V_E - I_2 R_S - L_S \frac{dI_2}{dt} - I_L R_L - L \frac{dI_L}{dt} = 0 \quad (16)$$

$$I - I_V - I_2 - C_m \frac{dV_E}{dt} = 0 \quad (17)$$

$$I_2 - I_L - C_P \frac{dV_L}{dt} = 0 \quad (18)$$

$$I_2 = 0 \quad (19)$$

$$I - I_V - C_m \frac{dV_E}{dt} = 0 \quad (20)$$

where, V_E is the residual voltage across the MOV. Equations (4), (5) and (14)-(18) represents the S_1 *ON* - S_2 *OFF* state of the circuit, whereas equations (4), (7)-(8), (14)-(15) and (19)-(20) are valid for the S_1 *OFF* - S_2 *ON* state of the circuit. In analogy with the section III-A, equations (14)-(20) can then be discretized using the Crank Nicholson algorithm in a *FDTD* scheme. The solution of the system yields the values of seven quantities I, I_2, I_V, I_L, V_E, V_L and V_C. The other quantities viz. the voltage across the switches, and the current passing through them can be deduced from them.

B. State Space approach to simulate the Power Converter protected by MOV

The approach is very similar to the one shown in Sec. III, the MOV device has been represented as the parallel connection of an ideal capacitor C_m and a non-linear resistor R_m. The relationship shown in (13) is not suitable for formulating the state equations. The non-linear resistor is used in a *KCL* to compute the instantaneous current on the capacitor. Since R_m is represented as a current-controlled resistor, using it to formulate the *KCL* would yield an implicit equation. Solving these equations would increase the computational time and may introduce convergence problems. Therefore, the R_m component is represented as a voltage-controlled current source as follows.

$$V_E = I_V \cdot R_m$$

$$I_V = \left(\frac{V_E}{K_i \cdot V_{ref} \cdot \left(1 / I_{ref}\right)^g} \right)^g \quad (21)$$

where the parameter g in (21) is same as the one mentioned in (13). K and α reported in Table III are still valid in the boundaries of the voltage V_E. The circuit is analogous to that shown in Fig. 2 with the MOV connected between A and B.

To reduce the computational complexity and to avoid divergences, the connecting wires parasitic inductance L_i was neglected. States S_1 *ON* and S_1 *OFF* state equations are

$$S_1\,ON: \begin{cases} \dot{x}_1 = \frac{1}{C}\left(-\frac{x_1}{R} - I_D\right) \\ \dot{x}_2 = \frac{1}{L}\left(x_3 - R_L x_2\right) \\ \dot{x}_3 = \frac{1}{C_P}\left(x_4 - x_2 + I_D\right) \\ \dot{x}_4 = \frac{1}{L_S}\left(-R_S x_4 - x_3 + x_5\right) \\ \dot{x}_5 = \frac{1}{C_m}\left(I_V + \frac{V_{in} - x_5}{R_i} - x_4\right) \end{cases} \quad S_1\,OFF: \begin{cases} \dot{x}_1 = \frac{1}{C}\left(-\frac{x_1}{R} - I_D\right) \\ \dot{x}_2 = \frac{1}{L}\left(x_3 - R_L x_2\right) \\ \dot{x}_3 = \frac{1}{C_P}\left(-x_2 + I_D\right) \\ \dot{x}_5 = \frac{1}{C_m}\left(I_V + \frac{V_{in} - x_5}{R_i}\right) \end{cases} \quad (22)$$

The new state variable x_5, is the voltage across the parasitic capacitance C_m of the MOV. In the S_1 *OFF* condition the x_4 state

variable (current on the parasitic inductance of the switch) is forced to zero, thus the relative state equation is not necessary.

C. Computations and Results

The MOV required to establish a desired protection level in the power converter is mainly guided by the absolute maximum ratings of the constituent elements viz. MOSFET, Diode, Capacitor, and the BUBO Inductor. The MOV with the lower clamping voltage and the highest possible current rating is selected for the converter used in this study. Figures 7, 8 and 9 represent the transients appearing across the components of the converter protected by MOV. The transient has been lowered to the extent depending upon the clamping voltage of the MOV. The comparison of the results shown in Figs. 4, 5 and 6 with those shown in Figs. 7, 8 and 9, respectively, is useful to comprehend the MOV effectiveness in lowering the converter component transient overvoltage/overcurrent.

The current sinking in the MOV during the lightning stroke is shown in Fig. 10. Almost the entire short circuit current provided by the Lightning Generator (LG) is taken by the MOV. The lifecycle of the MOV itself highly depends on the amplitude and duration of the current passing through it. The MOV manufacturers provide their derating curves indicating the lifetime of MOV, which is the number of strokes of a current pulse of a given amplitude and duration that the varistor can withstand without getting destroyed.

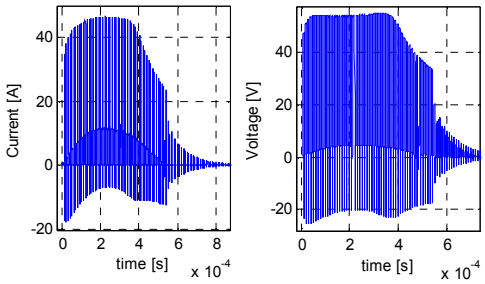

Fig. 7. Mosfet current (left) and Mosfet voltage (right) protected by MOV during the level transient waveform 5A/5A level 4.

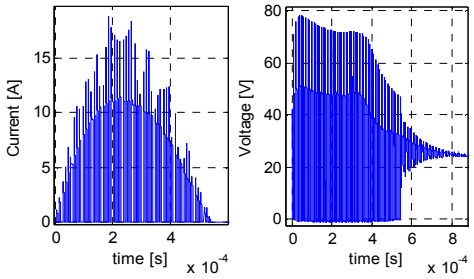

Fig. 8. Diode current (left) and Diode voltage (right) protected by MOV during the transient waveform 5A/5A level 4.

The numbers of strokes are defined for the rectangular type current pulses in the varistor datasheet, so it is necessary to convert MOV other wave shaped currents into rectangular equivalent type pulses to determine the varistor lifecycle [27]. The technique proposed by datasheets is explained in the Fig.10. This 700A, 85µs current pulse can destroy the varistor used in this simulation (see table III) within one to two strokes [25]. One approach to solve this problem would be to reduce the MOV current by using a higher clamping voltage MOV, but it will increase the residual voltage, which, in-turn, lowers the safety margin available for the converter components.

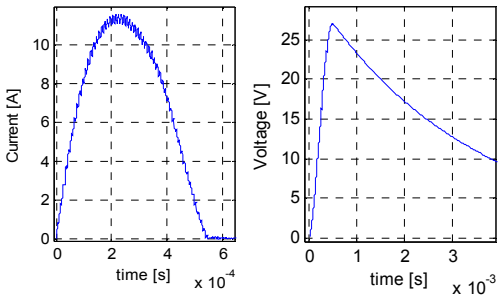

Fig. 9. BUBO inductor current (left) and output capacitor voltage (right) protected by MOV during the transient waveform 5A/5A level 4.

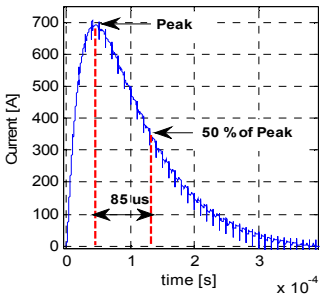

Fig. 10. MOV current during the transient Waveform 5A/5A, level 4.

Another way to improve the service life is by using the parallel combination of MOVs to share the current equally among them. The manufacturer specifies the tolerance level in the clamping voltage for each varistor, which means that it is impossible to manufacture identical twin Varistors. During the parallel operation, one can turn on sooner than the other. This causes the unequal sharing of current among the MOVs and might even cause a single varistor to take all the currents [27]. There is also a practice to use a series insertion resistor along with only one MOV. The problem with the series resistor is the insertion loss, as it must handle the entire normal load current. The use of series inductor in the place of a series resistor with the MOV is a better solution to the problem. The BI has been combined with a MOV to protect, in general, an Equipment Under Test in DC power lines in [21]. The BI has negligible insertion loss and has been already used as an effective solution to dampen the transients in power transmission lines. The transient wave is dampened to certain extent by a BI due to which, the MOV must handle reduced amplitude of the transient wave. Taking a cue from the above-mentioned facts, section V presents the modelling details and the simulation of the power converter protected by the series inductor BI and the MOV. The physical model of the series inductor is based on the geometrical parameters of the core, which makes it useful for the design of the core for the desired applications.

V. MOV AND BI FOR ROBUST AND RELIABLE PROTECTION OF THE POWER CONVERTERS

The BI selected for this study purposes is an inductor with a toroidal ferromagnetic core as shown in Fig.11 (i). The core consists of thin laminated tape of silicon iron alloy having a non-oriented grain (NOG) structure. For the condition depicted in Fig. 11 (ii), the magnetic field H has nonzero H_Z component along z-direction, and it is uniform along the x-direction.

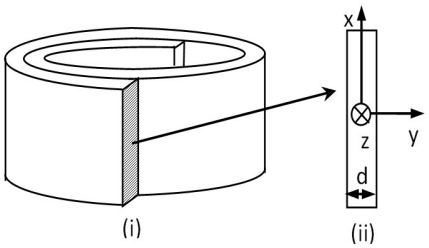

Fig. 11. (i) Qualitative picture of the toroidal ferromagnetic core of the inductor, (ii) Cross section area of the ferromagnetic sheet.

The propagation of magnetic field H in the core can be modelled by the diffusion equation

$$\frac{\partial^2 H_z}{\partial y^2} = \sigma\,\mu_0\left(1+\frac{dM_z}{dH_z}\right)\frac{\partial H_z}{\partial t} \tag{23}$$

where, M_Z is the non-zero component of the magnetization along z direction. The initial conditions and the boundary conditions required to solve (23) are

$$H_z(y,0)=0;\; M_z(y,0)=0;\; \left.\frac{dM_z}{dH_z}\right|_{t=0} = D_0 \tag{24}$$

$$H_z\left(\frac{b}{2},t\right) = H_{ext} = \frac{NI}{l};\qquad \left.\frac{\partial H_z}{\partial y}\right|_{y=0} = 0 \tag{25}$$

where D_0 is the initial value of the magnetization derivative and it is determined by using the measured virgin curve of the material. The diffusion equation (23) has the second order derivative in space and the first order derivative in time. The thickness b of the lamination sheet is discretized in m_{max} number of points along the direction y to solve (23). More details about the modelling of the ferromagnetic core inductor using the diffusion equation can be found in [21]. The paper here presents the implementation of that formulation for the proposed DC-DC power converter. The Fig. 12 shows the circuit of the converter protected by MOV and a series blocking inductor. In analogy with the previous sections, the Crank-Nicholson discretization in FDTD can be used to solve the diffusion equation of (23) and gives

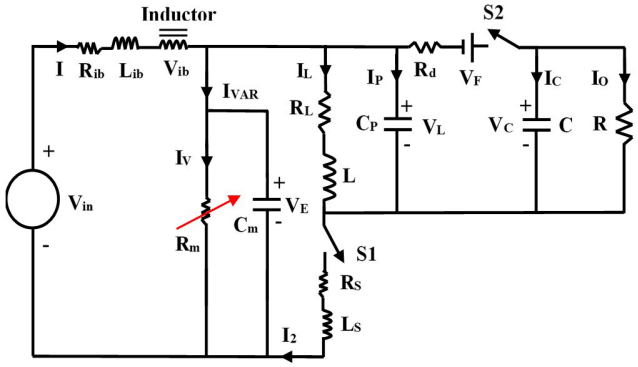

Fig. 12. Circuit utilized to study the MOV and the series inductor performances to protect the converter from indirect lightning.

$$\frac{1}{\Delta y^2}\left(H_1^{n+1}-H_0^{n+1}\right)-\frac{\sigma\mu_0}{\Delta t}\left(1+\left.\frac{dM}{dH}\right|_0^n\right)H_0^{n+1} = \frac{1}{\Delta y^2}\left(H_0^n-H_1^n\right)-\frac{\sigma\mu_0}{\Delta t}\left(1+\left.\frac{dM}{dH}\right|_0^n\right)H_0^n \tag{26}$$

$$\frac{1}{2\Delta y^2}\left(H_{m+1}^{n+1}-2H_m^{n+1}+H_{m-1}^{n+1}\right)-\frac{\sigma\mu_0}{\Delta t}\left(1+\left.\frac{dM}{dH}\right|_m^n\right)H_m^{n+1} = \frac{1}{2\Delta y^2}\left(2H_m^n-H_{m+1}^n-H_{m-1}^n\right)-\frac{\sigma\mu_0}{\Delta t}\left(1+\left.\frac{dM}{dH}\right|_m^n\right)H_m^n \tag{27}$$

where, n is the time step number, m is the space step number along the y-axis, σ is the electrical conductivity of the ferromagnetic core, μ_o is the vacuum magnetic permeability, M is the magnetization. Discretization of (23) results in (26) m=0, and (27) for all other steps excluding m=0 and m_{max}, where m_{max} is the total number of space steps. The other necessary equations result from the application of Kirchhoff's volt-amp balance equations in the circuit shown in Fig. 12, and are

$$-\left\{\left(0.5R_{ib}+\frac{L_{ib}}{\Delta t}\right)\frac{l}{N}+\left(\frac{\mu_o N n_s d a}{(m_{\max}+1)\Delta t}\right)\left(1+\left.\frac{dM}{dH}\right|_{m_{\max}}\right)\right\}H_{ext}^{n+1} -(0.5R_m)I_V^{n+1}-\left(\frac{\mu_o N n_s d a}{(m_{\max}+1)\Delta t}\right)\left\{\sum_{k=0}^{m_{\max}-1}\left(1+\left.\frac{dM}{dH}\right|_k\right)H_k^{n+1}\right\} = \left\{\left(0.5R_{ib}-\frac{L_{ib}}{\Delta t}\right)\frac{l}{N}-\left(\frac{\mu_o N n_s d a}{(m_{\max}+1)\Delta t}\right)\left(1+\left.\frac{dM}{dH}\right|_{m_{\max}}\right)\right\}H_{ext}^{n} +(0.5R_m)I_V^n-\left(\frac{\mu_o N n_s d a}{(m_{\max}+1)\Delta t}\right)\left\{\sum_{k=0}^{m_{\max}-1}\left(1+\left.\frac{dM}{dH}\right|_k\right)H_k^n\right\}-\left(\frac{V_{in}^{n+1}+V_{in}^n}{2}\right) \tag{28}$$

$$(0.5*R_m)I_V^{n+1}-0.5V_E^{n+1} = -(0.5*R_m)I_V^n+0.5V_E^n \tag{29}$$

$$-\left(0.5*R_S+\frac{L_S}{\Delta t}\right)I_2^{n+1}-\left(0.5*R_L+\frac{L}{\Delta t}\right)I_L^{n+1}+0.5V_E^{n+1} = \left(0.5*R_S-\frac{L_S}{\Delta t}\right)I_2^n+\left(0.5*R_L-\frac{L}{\Delta t}\right)I_L^n-0.5V_E^n \tag{30}$$

$$-\left(0.5*R_L+\frac{L}{\Delta t}\right)I_L^{n+1}+0.5V_L^{n+1} = \left(0.5*R_L-\frac{L}{\Delta t}\right)I_L^n-0.5V_L^n \tag{31}$$

$$0.5I_2^{n+1}-0.5I_L^{n+1}-\frac{C_P}{\Delta t}V_L^{n+1} = -0.5I_2^n+0.5I_L^n-\frac{C_P}{\Delta t}V_L^n \tag{32}$$

$$0.5*\left(\frac{l}{N}\right)H_{ext}^{n+1}-0.5I_V^{n+1}-\frac{C_m}{\Delta t}V_E^{n+1}-0.5I_2^{n+1} = -0.5*\left(\frac{l}{N}\right)H_{ext}^{n}+0.5I_V^n-\frac{C_m}{\Delta t}V_E^n+0.5I_2^n \tag{33}$$

$$\left(\frac{R*C}{\Delta t}+0.5\right)V_C^{n+1} = \left(\frac{R*C}{\Delta t}-0.5\right)V_C^n \tag{34}$$

$$-0.5*R_d I_L^{n+1}+0.5V_C^{n+1}-\left(0.5+\frac{R_d*C_P}{\Delta t}\right)V_L^{n+1} = 0.5*R_d I_L^n-0.5V_C^n+\left(0.5-\frac{R_d*C_P}{\Delta t}\right)V_L^n+V_F \tag{35}$$

$$\left(\frac{R*C}{\Delta t}+0.5\right)V_C^{n+1}+0.5*RI_L^{n+1}+\frac{R*C_P}{\Delta t}V_L^{n+1} = \left(\frac{R*C}{\Delta t}-0.5\right)V_C^n-0.5*RI_L^n+\frac{R*C_P}{\Delta t}V_L^n \tag{36}$$

$$I_2^{n+1} = 0 \tag{37}$$

$$0.5*\left(\frac{l}{N}\right)H_{ext}^{n+1}-0.5I_V^{n+1}-\frac{C_m}{\Delta t}V_E^{n+1} = -0.5*\left(\frac{l}{N}\right)H_{ext}^{n}+0.5I_V^n-\frac{C_m}{\Delta t}V_E^n \tag{38}$$

where R_{ib} is the sum of R_i and the BI winding resistance, L_{ib} is the sum of L_i and the BI leakage inductance, l is the average length of the toroidal core, N is the number of turns in the winding of the BI, n_s is the number of laminated rings in the BI core, d is the

This article has been accepted for publication in a future issue of this journal, but has not been fully edited. Content may change prior to final publication. Citation information: DOI 10.1109/TIE.2020.3013794, IEEE Transactions on Industrial Electronics

thickness of the lamination sheet, a is the width of the Lamination Sheet, and H_{ext} is the magnetic field at the surface of the lamination sheet. In our application, we are dealing with the unipolar double exponential transient waves. The magnetization behaviour of the core material under these circumstances can be accurately incorporated by considering the core anhysteretic behavior representation, which can be modelled according to

$$M = a \tan^{-1}(bH) + cH \quad (39)$$

where parameters a, b and c define the shape of the anhysteretic curve and are calculated from the series of measurements applying certain optimization technique viz. least square error method [28]. Values of the parameters a, b and c are given in Table IV. The S_1 *ON* - S_2 *OFF* state of the converter reported in Fig. 12 can be simulated by solving the system of equations (26)-(34). The S_1 OFF - S_2 ON state of the converter reported in Fig. 12 can be simulated by solving the system of equations (26)-(31) and (35)-(38). The solution of (26)-(28) gives H for $m=0$ to m_{max} points in the lamination sheet of the series inductor. The current I is evaluated from H_{ext} by using (25). The quantities along the converter components can be evaluated accordingly after the solution. The current in the MOV after the use of the series blocking inductor is reported in Fig.13. The current through the MOV is reduced from 700A to 450A for the level 4 amplitude of the waveform 5A (see Fig.10). The MOV used in this simulation can withstand the 105 μs current pulse of 450A for up to 15 strokes [25]. The MOV current reduction amount depends on the size of the series blocking inductor. The parameters of the series blocking inductor are reported in Table IV. The model of BI-MOV combination is also based on the geometrical parameters of the BI core, so it helps in the optimal design of BI to save the space and payload onboard. A suitable design procedure is the following: a) define the maximum cross section area A_{max} of the BI core; b) define the maximum value for the mean length l_{max} of the BI core; c) define the maximum BI weight w_{max}; d) select the BI wire with a cross section S corresponding to the nominal EUT current; e) determine the initial guess for the number of turns N using the relation $N = (B_{max} \cdot l_{max})/(I_{max} \cdot \mu_{lin})$ where B_{max} ≈1.6-1.7 T to avoid deep saturation, I_{max} is the maximum current of the selected MOV, μ_{lin} is the magnetic permeability of the BI core in the linear part of the anhysteretic curve; f) determine the initial guess for a, d and n_s using the relation $w_{max} = A_{max} \cdot l_{max} \cdot \rho_{Fe} + 2 \cdot (a + d \cdot n_s) \cdot N \cdot S \cdot \rho_{Cu}$, where ρ_{Fe} and ρ_{Cu} are the iron and copper density; g) utilize the numerical model presented in this paper, implemented in a recursive optimization procedure, to determine the best values of N, a, d, and n_s. The goal is to minimize the BI volume and weight, and DC-DC converter voltages and currents during the lightning strokes. In the recursive optimization procedure, the initial values of the parameters are defined in e) and f).

I. Experimental Validation for the Reliability Assessment of the Numerical Simulations.

The results predicted by the simulations were validated by experimental tests to demonstrate the viability of the protection system and the adopted modelling technique.

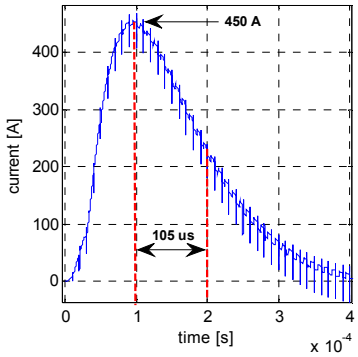

Fig. 13. Current through the MOV in the presence of series blocking inductor during the level 4 amplitude transient of the waveform 5A/5A.

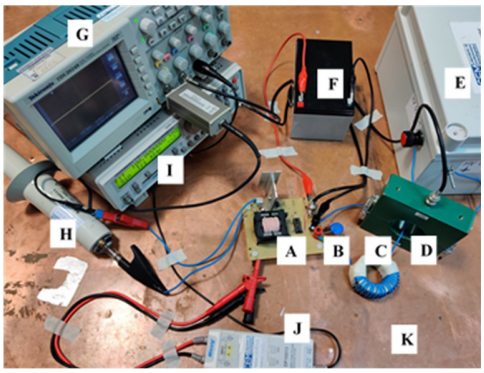

Fig. 14. The prototype and the experimental setup to validate the simulation results.

The prototype and the experimental setup is shown in Fig. 14, where A is the BUBO converter prototype, which was realized using the components shown in Table I, B-C are the combined MOV-BI, D is the 3525 Pearson Electronics current probe with a 5 Hz - 15 MHz bandwidth, 0.1 Volts per Ampere sensitivity, E is the lightning generator, F is the BUBO power MOSFET driver circuit power supply, G is the Tektronix TDS 2024B digital oscilloscope having a 200 MHz bandwidth and 2 GS/s sample rate, H is the P6015 Tektronix voltage probe having attenuation ratio 1000, I is the HAMEG HM8131-2 signal generator providing the PWM signal to the power MOSFET drive, J is the Micsig DP10013 high voltage differential probe with a 100 MHz bandwidth measuring the voltages across the diode and MOSFET, and K is the ground plane. Two lightning generators were used to generate waveforms 4/1 and 5A/5A as shown in Fig. 15.

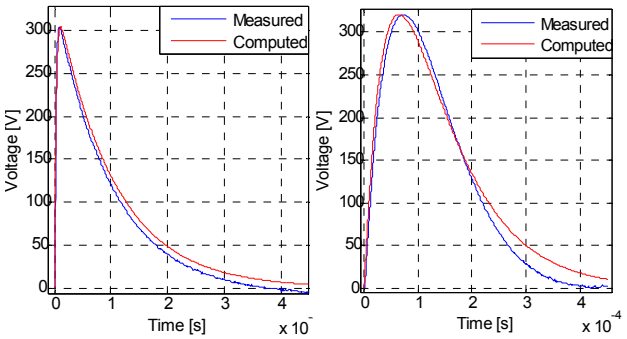

Fig. 15. Simulated and measured open circuit voltage generated by the LG for the level 3 amplitude of waveform 4/1 (left) and waveform 5A(right).

This article has been accepted for publication in a future issue of this journal, but has not been fully edited. Content may change prior to final publication. Citation information: DOI 10.1109/TIE.2020.3013794, IEEE Transactions on Industrial Electronics

A. Reliability Assessment for the Converter Normal Operation.

The measurements were performed at different duty ratios to evaluate the converter performance during the normal operation. Fig.16 reports a comparison between the simulated and measured waveforms of V_C at D=0.8. This voltage starting transient the steady-state values obtained from four different simulation approaches are compared with that measured. Measured waveform shows some oscillations, which are due to parasitic elements neglected in the converter model. The simulated results are in a good agreement with those resulting from measurement.

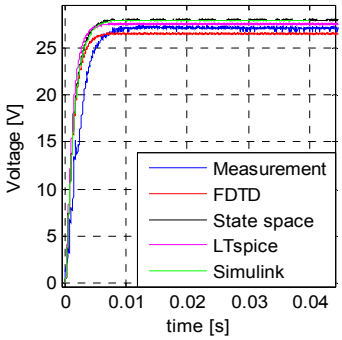

Fig. 16. Simulated and measured starting transient behavior of the converter output voltage for the 80% duty ratio.

B. Reliability Assessment for the Converter Protected by MOV.

The lightning waveforms 4/1 and 5A/5A were applied to the converter protected by MOV at the input terminals. The measurements were made at D=0.5 and at different amplitude levels of the lightning waveforms. To evaluate the computation accuracy and reliability, a comparison between the numerical schemes presented above, the commercial software, and the measurements are given. Fig.17 shows a comparison of the indirect lightning voltage waveform 5A/5A. The lightning pulse was applied to the BUBO circuit protected by MOV. The several computational approach results and measurements are in a good agreement. Figures 18 and 19 present the computed and the measured voltages across the diode terminals for the level 3 amplitude of the waveform 5A/5A, and the MOSFET for the level 3 amplitude of the waveform 4/1, respectively. The FDTD simulations results are a good estimation of those measured.

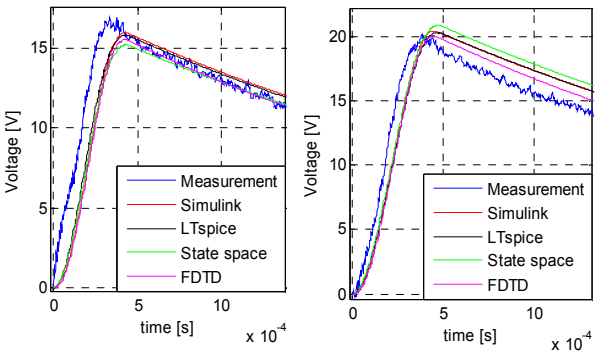

Fig. 17. Simulated and measured voltage V_c in the BUBO circuit protected by MOV for the waveform 5A/5A level 2 (left), level 3 (right).

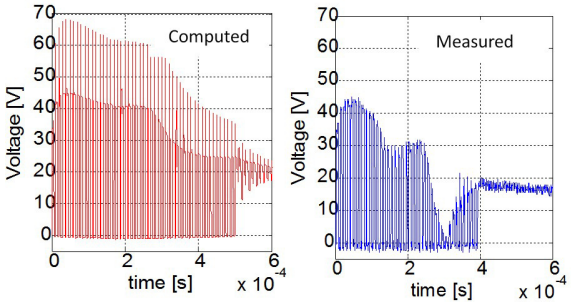

Fig. 18. Computed and measured diode voltage for the waveform 5A/5A level 3 in the BUBO circuit protected by MOV.

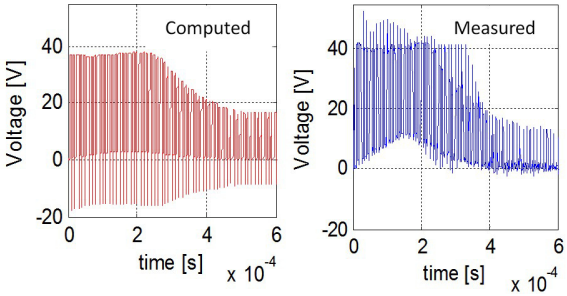

Fig. 19. Computed and measured Mosfet voltage for the waveform 4/1 level 3 in the in the BUBO circuit protected by MOV.

C. Reliability Assessment for the Converter Protected by Series Blocking Inductor and MOV.

The waveforms 4/1 and 5A/5A were applied to the converter protected by the series blocking inductor and the MOV (see Fig. 12). The tests were done at a D=0.5. The comparison between the simulated and measured output capacitor voltages for 2, 3 and 4 amplitude levels of the waveform 5A/5A are reported in the Fig. 20. The total currents I for the same three levels are shown in Fig. 21. Similarly, Figs. 22, 23 and 24 reports the same two quantities, I and V_C at the amplitude levels 1, 2 and 3 of waveform 4/1. Apart from some minor deviation in the quantity V_C for some levels, the simulation and measurement results are in good. Figures 25 and 26 present the computed and the measured diode voltages for level 3 amplitude of waveform 4/1 and the MOSFET voltages for level 3 amplitude of waveform 5A/5A, respectively. Voltages and currents estimations are quite accurate. The simulations and measurements have been performed upto level 4 amplitude of waveform 4/1 and waveform 5A/5A. The results for some amplitude levels have been reported in the paper keeping in mind the available paper maximum length. Table V reports an easy comparison of results for different protection schemes studied in this paper.

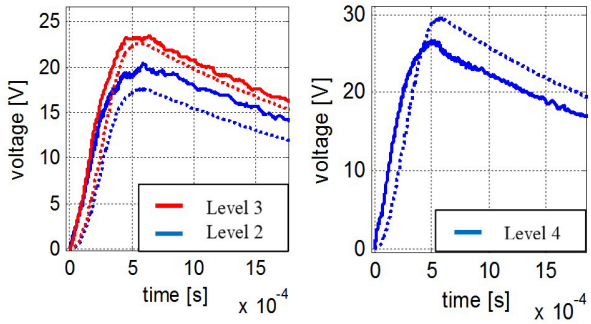

Fig. 20. Comparison of the computed (dotted line) and measured (solid line) voltage V_c (see Fig.12) for 3 amplitudes of the WF 5A/5A.

This article has been accepted for publication in a future issue of this journal, but has not been fully edited. Content may change prior to final publication. Citation information: DOI 10.1109/TIE.2020.3013794, IEEE Transactions on Industrial Electronics

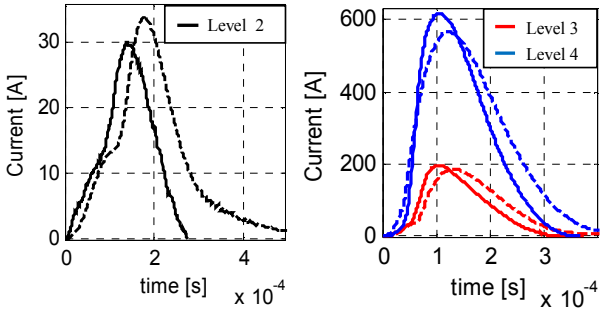

Fig. 21. Comparison of the computed (dotted line) and measured (solid line) current I (see Fig.12) for 3 amplitudes of the waveform 5A/5A.

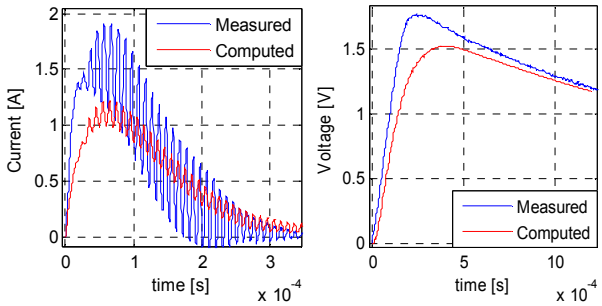

Fig. 22. Computed and measured current I (left) and voltage V_c (right) for level 1 amplitude of the waveform 4/1 in the circuit of Fig.12.

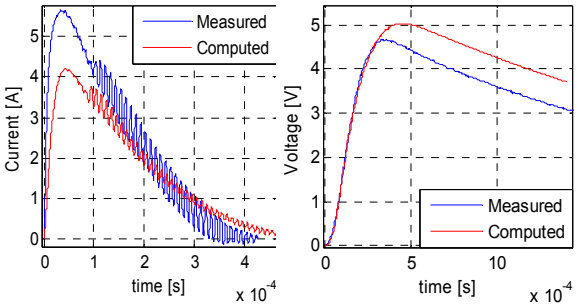

Fig. 23. Current I (left) and voltage V_c (right) for WF4/1 level 2 (Fig.12)

The quantities trend shown in Table V is consistent for all the other lightning waveforms amplitude. The high frequency switching action of the DC-DC converter during its operation results in erratic and chopped MOSFET and diode voltages. These waveforms are highly sensitive to the circuit parasitic elements. An accurate modelling of parasitic components for circuit simultaions is cumbersome, this is the reason why it is difficult to match MOSFET and diode voltage waveforms amplitude with its exact wave shape. The calculated and measured diode and Mosfet voltages in figures 18, 19, 25 and 26 are consistent in terms of their amplitude and slightly different in terms of their wave shapes. Maximum value accuraret prediction and waveform envelopes with the same order of magnitude can be assumed as satisfactory results. The maximum value is significative, because it is important to identify a possible breakdown. A small errors in estimating the B-H operating point from the hysteresis model, and the V-I operating point from the MOV model also contribute to the difference between simulated and measured results.

I. CONCLUSION

A model of a DC-DC converter, useful to design a suitable lightning transient protection system for avionic application, has been discussed in the paper.

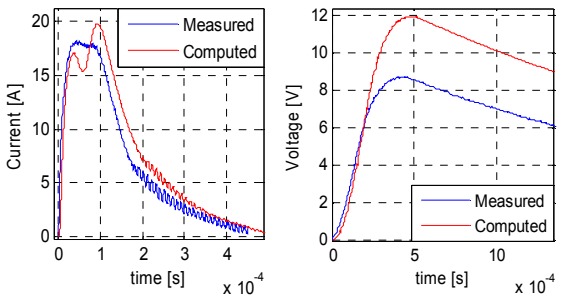

Fig. 24. Current I (left) and voltage V_c (right) for WF4/1 level 3 (Fig.12)

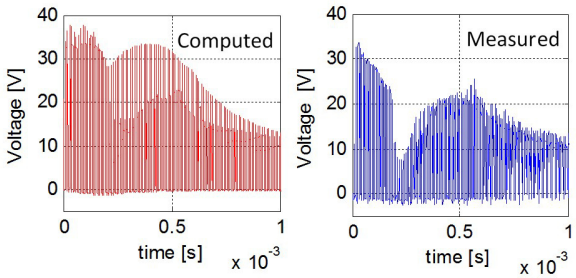

Fig. 25. Computed and measured diode voltage for level 3 amplitude of the waveform 4/1 in the circuit of Fig.12.

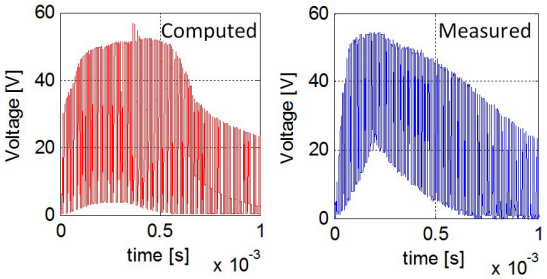

Fig. 26. Computed and measured Mosfet voltage for level 3 amplitude of the waveform 5A/5A in the circuit of Fig.12.

A PWM DC-DC Buck-Boost converter has been selected. The model also incorporates the parasitic elements of the converter circuit. The combination of a MOV and a series blocking inductor to provide robust and reliable protection to the converter from lightning indirect effects in avionic environment has been considered. The proposed protection system, along with the converter has been modelled using an equivalent circuital approach and the magnetic diffusion equation in one dimension. The magnetization process of the series inductor core material has been modelled using the experimental virgin curve. The numerical computations have been done using a Crank-Nicholson approach in FDTD scheme. The computation results for some of the analyzed cases have been verified by using a) the State Space Approach, b) MATLAB/SIMULINK©, c) LTspice©. The good agreement between the simulated and measured results for all the examined cases, for different amplitude levels of different indirect lightning overvoltage waveforms, indicates the practical efficiency and usability of the proposed model when applied to a real power converter, updating previous validation of the model which was achieved only on linear time-invariant circuits. The paper also deals with practical issues regarding the protection of sensitive low voltage avionic equipment from very high voltage lightning transients. The analysis presented here, for an open loop controlled converter, is also valid and useful for the closed loop control. Since the lightning waveforms defined by the standards are relatively short duration transients, the frequency contents of such waveforms are up to the range of several

hundreds of kHz, and such frequency range is usually greater than the crossover frequency of the closed loop system. As a consequence, the controller may not be able to attenuate such frequencies arriving at the input terminals of the converter during the lighting events [29]. However, this issue deserves further investigations that can be an interesting starting point for a future work. Further possible developments consist in the application of the proposed protection method to other DC-DC converter topologies and its investigation in converters operating under discontinuous conduction mode.

TABLE I
PARAMETERS OF THE BUBO CONVERTER FOR NORMAL OPERATION

Parameter	Value
BUBO Inductor resistance (R_L)	0.991 Ω
BUBO Inductor Inductance (L)	240 μH
BUBO Inductor parasitic capacitance (C_P)	20 nF
Output capacitor capacitance (C)	66.5 μF
BUBO load resistor resistance (R)	50 Ω
MOSFET conducting resistance (R_S)	0.4 Ω
MOSFET turn on inductance (L_S)	20 nH
Diode conducting resistance (R_d)	0.05 Ω
Diode forward voltage drop (V_F)	0.5 V
MOSFET Switching frequency	100 kHz
Input voltage (V_{in})	12 V
Internal resistance of the voltage source (R_i)	65 mΩ
Parasitic Inductance of the connecting wires (L_i)	1 nH

TABLE II
PARAMETERS TO MODEL THE LIGHTNING WAVEFORMS

Parameter	Waveform 4/1	Waveform 5A/5A
Equation for $V_{in}(t)$	K [exp(-αt)-exp(-βt)]	K [exp(-αt)-exp(-βt)]
α	9600	10300
β	320000	41000
K for level 1	58	142
K for level 2	145	303
K for level 3	363	690
K for level 4	827	1585
Internal resistance (R_i)	5 Ω	1Ω
Parasitic Inductance (L_i)	1 nH	1nH

TABLE III
PARAMETERS TO SIMULATE THE MOV

Parameter	Value
Manufacturer	EPCOS©
Reference voltage (V_{ref})	15.73 V
Reference current (I_{ref})	1 mA
$\alpha_1 = 2.4448$; $K_1 = 1$	$0 \le I < 1$ mA; $0 \le V_E < 15.73$ V
$\alpha_2 = 12.5471$; $K_2 = 1$	$1\text{mA} \le I < 114.2$ A; $15.73 \le V_E < 40.74$ V
$\alpha_3 = 6.9689$; $K_3 = 0.4870$	$I \ge 114.2$ A; $V_E \ge 40.74$ V
Parasitic Capacitance (C_m)	23000×10^{-11} F

TABLE IV
PARAMETERS OF THE SERIES BLOCKING INDUCTOR

Parameter	Value
Number of turns (N)	24
Winding Resistance (Rib)	0.04 Ω
Number of core lamina	43
Leakage Inductance (Lib)	10 μH
Width of the laminated sheet (w)	1 cm
Thickness of the laminated sheet (b)	0.65 mm
Inner radius of the toroidal core	2 cm
Outer radius of the toroidal core	3 cm
Conductivity of the iron core (σ)	$1.8 \cdot 10^6$ S/m
Parameters of the anhysteretic curve	a=0.929, b=$0.335 \cdot 10^{-2}$, c=$0.305 \cdot 10^{-4}$.

TABLE V
COMPARISON OF RESULTS FOR DIFFERENT PROTECTION SCHEME

Parameter	No Protection	Protected by MOV	Protected by MOV-BI
MOV Current	-	700 A	450 A
Mosfet Voltage	750 V	60 V	85 V
Diode Voltage	710 V	75 V	80 V
Capacitor Voltage	160 V	27 V	30 V

REFERENCES

[1] J. A Rosero, J. A. Ortega, E. Aldabas, and L. Romeral, "Moving towards a more electric aircraft," *IEEE Aerosp. Electron. Syst. Mag.*, vol. 22, No. 3, pp. 3–9, Mar. 2007.

[2] B. Axelrod, Y. Berkovich, A. Ioinoivici, "Switched-capacitor/switched-inductor structures for getting transformerless hybrid DC-DC PWM converters", (2008) *IEEE Transactions on Circuits and Systems I: Regular Papers*, Vol. 55, No. 2, pp. 687-696, 2008.

[3] B. J. Patella, A. Prodić, A. Zirger, D. Maksimović, "High-frequency digital PWM controller IC for DC-DC converters" *IEEE Transactions on Power Electronics*, Vol. 18, No. 1 II, pp. 438-446, 2003.

[4] L. Zhu, "A Novel soft-commutating isolated boost full-bridge ZVS-PWM DC-DC converter for bidirectional high-power applications", *IEEE Transactions on Power Electronics*, Vol. 21, No. 2, pp. 422-429, 2006.

[5] Y. M. Chen, Y. C. Liu, F.Y. Wu, "Multi-input dc/dc converter based on the multiwinding transformer for renewable energy applications", *IEEE Transactions on Industry Applications*, Vol. 38, No. 4, pp. 1096-1104, 2002.

[6] Y. M. Chen, Y.C. Liu, S.H. Lin, "Double-input PWM DC/DC converter for high-/low-voltage sources", *IEEE Transactions on Industrial Electronics*, Vol. 53, No. 5, pp. 1538-1545, 2006.

[7] M. K. Kazimierczuk, "Pulse-width Modulated dc-dc Power Converters" in John Wiley & Sons, 2008.

[8] A. Ayachit, A. Reatti, M. K. Kazimierczuk, "Small-signal modeling of the PWM boost DC-DC converter at boundary-conduction mode by circuit averaging technique," Proceedings of EEE International Symposium on Circuits and Systems, ISCAS 2015, Lisbon, 24-27May 2015, pp. 229-232.

[9] A. Reatti, M. Balzani, "PWM switch model of a buck-boost converter operated under discontinuous conduction mode," Proceedings of IEEE International 48th Midwest Symposium on Circuits and Systems, MWSCAS 2005; Cincinnati, OH, USA, 7-10 August 2005, pp. 667-670.

[10] A. Luchetta, S. Manetti, M. C. Piccirilli, A. Reatti and M. K. Kazimierczuk, "Derivation of Network Functions for PWM DC-DC Buck Converter in DCM Including Effects of Parasitic Components on Diode Duty-Cycle", Proc. of IEEE 15th International Conference on Environment and Electrical Engineering, Rome, Italy, June 10th-13th 2015, pp. 778-783.

[11] M. Catelani, L. Ciani, A. Reatti, "Critical components test and reliability issues for Photovoltaic Inverter", Proceeding of 20th IMEKO TC-42014 – International Workshop on ADC and DAC Modelling and Testing, Benevento, Italy, September 17-17, 2014, pp. 592-596.

[12] Z. Zhao, M. Xu, Q. Chen, J. Lai, and Y. Cho, "Derivation, Analysis, and Implementation of a Boost–Buck Converter-Based High-Efficiency PV Inverter", *IEEE Transactions on Power Electronics*, Vol. 27, No. 3, March 2012.

[13] D. K. Saini, A. Ayachit, A. Reatti, M. K. Kazimierczuk, "Analysis and Design of Choke Inductors for Switched-Mode Power Inverters", *IEEE Transactions on Industrial Electronics*, Volume 65, No. 3, Pages 2234-2244, March 2018.

[14] L. Huang, C. Gao, F. Guo and C. Sun, "Lightning Indirect Effects on Helicopter: Numerical Simulation and Experiment Validation", IEEE Trans. on Electromagnetic Compatibility, vol. 59, No. 4, pp. 1171-1179, Aug. 2017.

[15] E. Perrin, C. Guiffaut, A. Reineix and F. Tristant, "Using a Design-of-Experiment Technique to Consider the Wire Harness Load Impedances in the FDTD Model of an Aircraft Struck by Lightning," *IEEE Transactions on Electromagnetic Compatibility*, vol. 55, No.. 4, pp. 747-753, Aug. 2013.

[16] Environmental Conditions and Test Procedures for Airborne Equipment, Standard RTCA/DO-160G, RTCA Inc. December 8, 2010.

[17] A. Luchetta, S. Manetti, M. C. Piccirilli, A. Reatti, F. Corti, M. Catelani, L. Ciani, M. K. Kazimierczuk, "MLMVNNN for Parameter Fault Detection in PWM DC-DC Converters and Its Applications for Buck and Boost DC-DC Converters", *IEEE Transactions on Instrumentation and Measurement*, Volume 68, No. 2, Pages 439-449, Feb 2019.

[18] B. Valecillos, and J. Ramirez, "Evaluation of Lightning Impulse Test by Frequency Response Analysis", 2006 IEEE PES Transmission and Distribution Conference and Exposition Latin America, Venezuela, 15-18 Aug. 2006, Caracas, Venezuela.
[19] C. Yajing, Z. Wenjun, H. Ruidong, Z. Luxing, "Test on Lightning Characteristics of Electronic Equipment's Power Supply", IEEE 2007 International Symposium on Microwave, Antenna, Propagation, and EMC Technologies For Wireless Communications, 16-17 Aug. 2007, Hangzhou, China.
[20] V.A Rakov, F. Rachidi, "Overview of recent progress in lightning research and lightning protection" *IEEE Transactions on Electromagnetic Compatibility*, Vol. 51, No. 3, pp. 428-442, 2009.
[21] A. Faba, H. Rimal, "Robust Lightning Indirect Effect Protection in Avionic Diagnostics: Combining Inductive Blocking Devices with Metal Oxide Varistors", IEEE Trans. on Ind. Electr., 65 (8), pp. 6457-6467, 2018.
[22] J. Crank, P. Nicolson, "A practical method for numerical evaluation of solutions of partial differential equations of the heat conduction type". Proc. Camb. Phil. Soc. 43 (1): 50-67, 1947.
[23] O. Clark, R. Gavender, "Lightning Protection for Microprocessor-Based Electronic Systems," *IEEE Trans. on Ind. Appl.,* Vol. 26, No. 5, pp. 947-953, 1990.
[24] I. A. Metwally, M. Eladawy, E. A. Feilat, "Online condition monitoring of surge arresters based on third-harmonic analysis of leakage current," *IEEE Trans. on Dielectrics and Electrical Ins.,* vol. 24, No. 4, pp. 2274-2281, 2017.
[25] EPCOS©, AG. "General technical information", SIOV metal oxide varistors, (2017). [Online]. Available: http://www.mouser.com
[26] MATLAB/SIMULINK©, "Documentation for the varistor". [Online]. Available: https://it.mathworks.com
[27] EPCOS©, AG. "Selection Procedure." SIOV metal oxide varistors, 2018. [Online]. Available: https://www.tdk-electronics.tdk.com
[28] F. C. Trutt, E. A. Erdelyi and R. E. Hopkins, "Representation of the Magnetization Characteristic of DC Machines for Computer Use," *IEEE Trans. on Power Apparatus and Systems*, vol. 87, No. 3, pp.665-669, 1968.
[29] Erickson, Robert W., and Dragan Maksimovic. *Fundamentals of power electronics*, Springer Science & Business Media, 2007.

Hari Prasad Rimal received the bachelor's degree in electrical engineering from the Institute of Engineering, Tribhuvan University (TU-IOE), Lalitpur, Nepal, in 2011, and the M. Sc. degree in electrical engineering from TU-IOE and Politecnico di Milano, Milan, Italy, in 2015. He obtained the Ph.D. degree in industrial engineering at the University of Perugia, Perugia, Italy, in 2020.
He is currently a post doctoral researcher at the same university. He is author of several scientific articles that are published in the reputed IEEE and Elsevier journal. He has been referee for some IEEE transactions and conference articles. His research interest include power electronics and the modeling and experimental characterization of magnetic materials.

Alberto Reatti (M'13) received the degree in electronics engineering from the University of Florence, Italy, in 1988, and the Ph.D. degree from the University of Bologna, Bologna, Italy, in 1993. In 1992, he was an Associate Researcher with the Department of Electrical Engineering, Wright State University, Dayton, OH, USA.
He is currently Associate Professor at the Department of Information Engineering since 2000 and president of Patent and Technology Transfer Board of University of Florence. He has co-authored more than 100 papers, including those appeared in IEEE Transactions and Journals. He holds two patents. His current research interests include high frequency resonant and PWM DC–DC power converters, modeling and control of converters, renewable power sources, energy saving, wireless power transfer, H2 storage, and reliability of switching power converters.

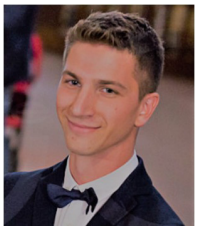

Fabio Corti received the M.S. degree in electrical and automation engineering and the PhD in industrial engineering from the University of Florence, Italy, in 2016 and 2019 respectively.
He is currently post-doctoral research fellow at Consiglio Nazionale delle Ricerche (CNR). His research interest includes modeling and control of DC-DC PWM and resonant converters, wireless power transfer and electric vehicle powertrain.

Gabriele Maria Lozito was born in Rome, Italy, in 1984. He received the master degree in Electronics Engineering from the University of Roma Tre in 2010, and the Ph.D. on Softcomputing Techniques on Embedded Systems from the University of Roma Tre in 2016.
He is currently a postdoc researcher at the University of Roma Tre on the main research topic of circuit modeling for renewable energy applications. His other areas of research includes machine learning and optimization algorithms, embedded devices implementations and magnetic materials modeling. He was visiting researcher at the National Physical Laboratory (NPL) in London. He served as chair in IEEE congresses and has published his research in several international journals including IEEE Transactions.

Simone Quondam Antonio graduated summa cum laude in Electronics and Communications Engineering from the University of Perugia, Italy, in 2014, and received the Ph.D. in Energy and Sustainable Development from the University of Perugia in 2018.
He is currently Post Doctoral Research Fellow at the Engineering Department of the University of Perugia, in the Centre for Magnetic Innovative Technologies, co-sponsored by Tamura Magnetic Engineering. His main scientific interests include the modelling of magnetic hysteresis for ferromagnetic materials, the experimental testing of magnetic components for industry and avionic applications. He served as chairman in several IEEE conferences. He also attended some IEEE conferences as invited speaker.

Antonio Faba received the Electrical Engineering Degree from the University of L'Aquila, Italy, in 1998, and the Ph.D. in Industrial Engineering from the University of Perugia, Italy, in 2006. He received the National Habilitation for Associate Professor in 2013, and the National Habilitation for Full Professor in 2018.
He is currently Assistant Professor with the Department of Engineering, University of Perugia, Italy, where he is the Head of the Laboratory of Electromagnetic Characterization. He is senior member of the IEEE Institute of Electric and Electronic Engineering and member of the IEEE Magnetic Society.

Ermanno Cardelli. Degree in Electrical Engineering at University of Pisa. Professional engineer. Ph.d. in Electrical Engineering at University of Pisa. Currently Full Professor of Electric Engineering at the University of Perugia, and Head of Department of Engineering. Senior Member IEEE. Past Chair of the IEEE Italy Section. Chair of the ElecTrical Engineering (ET) Group. Author of more than 200 refereed technical papers, mainly on numerical tecniques and modelling for the electromagnetic field analysis. Authors of two italian edited books and and of an international book chapter. Referee and guest editor for international journals. General Chair in several International Conferences. Coordinator of many Italian and European Scientific Programmes.